Gradient Characterization in Magnetic Resonance Imaging

by

Joseph Yitan Cheng

B.S. EECS, Massachusetts Institute of Technology, 2006

Submitted to the Department of Electrical Engineering and Computer Science
in partial fulfillment of the requirements for the degree of

Master of Engineering in Electrical Engineering and Computer Science

at the

MASSACHUSETTS INSTITUTE OF TECHNOLOGY

September 2007

Author .....
Department of Electrical Engineering and Computer Science
August 21, 2007

Certified by .....
Elfar Adalsteinsson
Assistant Professor of EECS & HST
Thesis Supervisor

Accepted by .....
Arthur C. Smith
Chairman, Department Committee on Graduate Students

Gradient Characterization in Magnetic Resonance Imaging

by

Joseph Yitan Cheng

Submitted to the Department of Electrical Engineering and Computer Science
on August 21, 2007, in partial fulfillment of the
requirements for the degree of
Master of Engineering in Electrical Engineering and Computer Science

Abstract

Special magnetic resonance (MR) scans, such as spiral imaging and echo-planar imaging, require speed and gradient accuracy while putting high demands on the MR gradient system that may cause gradient distortion. Additionally, high field MR scans are prone to inhomogeneities that disturb the gradient system. Regardless of the source, gradient characterization provides a simple tool for distortion correction. An improved method, named the self-encoded slice selection algorithm, of characterizing the gradient system of the magnetic resonance system is proposed. It improves and combines the self-encode method and the direct slice selection method. The new approach is simple and fast, and allows for the measurement of waveform gradients that reach the system's limits. The technique is used to model the gradient system as a linear time-invariant transfer function through frequency-domain analysis and time-domain analysis. A transfer function model of the gradient system on the 3T Siemens Tim Trio scanner is presented here along with the characterization and analysis of common waveform gradients. Possible distortion correction approaches are also suggested.

Thesis Supervisor: Elfar Adalsteinsson
Title: Assistant Professor of EECS & HST

Acknowledgments

I would like to thank my parents for instilling in me the love to learn and explore. I am thankful for all their encouragements and support throughout my education at MIT. I am quite grateful and honored to have the chance to work under Professor Adalsteinsson's supervision. A lot of this project is made possible through him, and I learned a lot through him. I thank my labmates for a fun environment to work in, Christina for providing all the Siemens MR scanner answers, the Martinos Imaging Center for letting me use the scanner, and all my friends who loved and cared for me. Lastly and most importantly, I would like to thank God for all the great opportunities that He has provided me here and the blessings He has already prepared for my future.

Contents

List of Figures

List of Tables

Chapter 1

Introduction

Of the major concerns of magnetic resonance (MR) studies, the work I present here will primarily address the issue of accuracy of data acquisition. More specifically, precise knowledge of data sample locations in the frequency k-space is crucial in MR scans. The accuracy of k-space locations, determined by waveforms applied by the gradient hardware system, will be the focus of this paper.

Modern MR scanners have developed a level of sophistication in which the majority of the inaccuracies associated with the k-space locations (notated with functions $k_x(t)$ and $k_y(t)$) is eliminated through methods such as B_0 shimming and eddy current suppression. However, if high enough demands are placed on the gradient hardware, the MR system may not properly correct these inaccuracies. Echo-planar imaging (EPI), spiral imaging, and other fast MR scans are examples of applications that may require the application of different waveform gradients that reach the MR system's limits. Additionally, there is an increasing interest in high field MR studies, such as scans with a main magnetic field of 7T. At these high fields, gradient distortion is an issue.

Gradient characterization provides a tool to measure actual k-space locations and to correct for any nonidealities caused by the scanner's hardware inadequacies in high fields or by the application of extreme waveform gradients. There is an assortment of different algorithms that can accomplish this task. In one such technique, the gradient system hardware can be modeled with inductors and resistors. Using the resulting simplified system, k-space trajectories can be designed to minimize the amount of inhomogeneities present in the scans [7]. Other proposed procedures steer away from modeling a specific scanner's

hardware and, instead, use the excitation of different phantoms, inanimate MR test objects usually filled with water, to characterize the waveform gradient. Point impulse samples of tap water (on the order of $20\mu l$) can be placed at different off-isocenter locations. The waveform gradient in question can be extracted from the acquired data after exciting the water samples and applying the test waveform gradient [5]. Other proposed methods use a large arbitrarily-shaped phantom. The phantom is scanned using special pulse sequencing designed to allow for easy extraction of the test waveform gradient through data processing [6] that often involves Fourier analysis [2] [4].

I propose a new method of gradient characterization, the self encoded slice selection algorithm, that is based on previous methods of arbitrarily-shaped phantom excitation. More specifically, it is an improvement of the self-encode method developed by Onodera *et al* [6] and of the direct slice selection method developed by Duyn *et al* [2]. The proposed algorithm is fast, robust, and flexible in measuring waveform gradients that put high demands on the MR gradient system.

Additionally, obtaining a gradient system transfer function through the use of previous gradient characterization method provides an even more general method of determining actual k-space trajectories [3]. Using the proposed technique, I will analyze the gradient system with a transfer function and provide test examples of commonly used waveform gradients: trapezoid gradient, spiral gradient, and EPI gradient.

Chapter 2

Method

To understand the methodology used for the different characterization algorithms, some background MR theory will be first presented in section 2.1. Next, in section 2.2, the self encode method [6] and the direct slice selection method [2] will be analyzed to aid in the explanation of the proposed self encoded slice excitation method. Lastly, the proposed technique will be applied in modeling the gradient system as a linear time-invariant transfer function using a frequency-domain approach and a time domain approach in section 2.3.

2.1 Background theory

Atoms with an odd number of protons or neutrons possess a nuclear spin angular momentum. MR studies consist of interacting with the spins of these atoms using different magnetic fields. Hydrogen is the most commonly used atom for its sensitivity to magnetic fields and its abundance in biological tissue.

The MR scan begins with a main magnetic B_0 field that is applied to the test subject. The B_0 field creates a net spin momentum aligned with field itself. The molecules then possess a resonance at a specific frequency (noted as the Larmor frequency). Next, a radiofrequency (RF) pulse, emitted from the transmitter coils and tuned to the Larmor frequency, is used to disturb the atoms of a designated slice. As the spins of the excited slice precess back to the B_0 field, gradients, $G(t)$, are applied, and the exponentially decaying signal is sampled through receiver coils. The magnetic spins decay with a time constant T_1 along the B_0 axis and a time constant of T_2 along the plane perpendicular to B_0.

The signal obtained through a T_1-weighted MR scan can be expressed with the approx-

imation:

$$s(t) = \int_y \int_x m(x,y) e^{i[2\pi k_x(t)x + 2\pi k_y(t)y + b(t)]} dxdy, \tag{2.1}$$

where $k_x(t)$ and $k_y(t)$ with corresponding $G_x(t)$ and $G_y(t)$ are defined by the following formula:

$$k(t) = \frac{\gamma}{2\pi} \int_0^t G(\tau) d\tau. \tag{2.2}$$

The quantity $m(x,y)$ is the spin magnetization that can be extracted using two dimensional Fourier transform analysis. The $m(x,y)$ signal can then be processed to produce the desired image or graph. The Fourier transform calculation requires accurate knowledge of $k_x(t)$ and $k_y(t)$, locations of samples in the Fourier transform of the signal, $\mathcal{FT}\{m(x,y)\}$. The problem being addressed by gradient characterization is the accuracy of this correspondence.

There are some MR specific terminology used throughout this paper. The sequence repetition time, TR, is the time between each RF excitation pulse. The gradient echo time, TE, is the time from the RF excitation pulse to when the read-out data is acquired. Additionally, k-space, with k_x, k_y, and k_z coordinates, is used to notate the MR Fourier-domain.

2.2 Gradient characterization methods

There exist many different methods that can characterize the gradients, $G(t)$, played by the gradient coils of the MR scanner. Additionally, from those methods, the actual k-space trajectory can be measured since the k-space trajectory is the integral of the characterized $G(t)$, as seen in equation 2.2.

For this thesis, procedures using an arbitrary phantom are analyzed and tested because these algorithms do not require detailed knowledge about the hardware of a specific scanner. Also, they do not need a unique hardware implementation or unique phantom construction for each measurement. The test waveform gradient in question can be characterized using a regular spherical phantom with standard receiver coils. In sections 2.2.1 and 2.2.2, I will describe techniques that were previously used along with their advantages and disadvantages. In section 2.2.3, I will propose a new method that makes use of both of the previous algorithms' advantages.

2.2.1 Self-encode method

Onodera *et al* proposed the self-encode gradient characterization method [6]. In this method, a large phantom is excited and a one-dimensional test gradient waveform is sent through the gradient coils. The waveform can be measured through post-processing of the acquired data.

Takahashi *et al* extended this algorithm to measure the gradients in two spatial dimensions. The measured data are then used to minimize waveform distortion and improve the excitation profile [8]. I used a variant of the procedure proposed by Takahashi *et al* for my analysis.

In the method of Takahashi *et al*, a slice of a large phantom is excited with a normal low flip RF pulse. The resulting signal will be the Fourier transform of the large excited phantom, which is a very narrow *sinc* function centered around the origin. Qualitatively speaking, the signal has a peak at the origin.

After the excitation pulse, a conventional phase-encode gradient (also known as "self-encode" gradient) is played out on the axis with the test waveform gradient in question. Since these self-encode gradients must be accurate and well-formed, they are designed to be well within the MR system's maximum gradient amplitude and maximum slew rate (how fast the gradient hardware is altering the gradient strength, $\frac{dG(t)}{dt}$). The self-encode gradients off-set the k-space location by a fixed amount: $k_{se}(n)$ for the n-th self-encode.

For the implementation of the self-encode algorithm, I create my own self-encode gradients to ensure I get the maximum resolution in the shortest amount of time. To do this, the maximum $k_{se}(n)$ offset is set to $k_{max}P_{se}$. The variable k_{max} is the maximum k-space point that the test waveform reaches, and the variable P_{se} is a scaling factor that increases the self-encode gradient amplitude to reach k-space points beyond k_{max}. The number of self-encode amplitudes, N_{se}, is a parameter that controls the resolution of the gradient characterization. The offset $k_{se}(n)$ can be expressed as

$$k_{se}(n) = k_{max} - n\left(\frac{2k_{max}P_{se}}{N_{se}-1}\right) \qquad \text{where } n = 0, 1, 2, \ldots N_{se} - 1. \tag{2.3}$$

After the self-encode gradient is played, the test waveform gradient $G(t)$ to be characterized is applied. For a general c-axis, the resulting k-space point at time t with self-encode

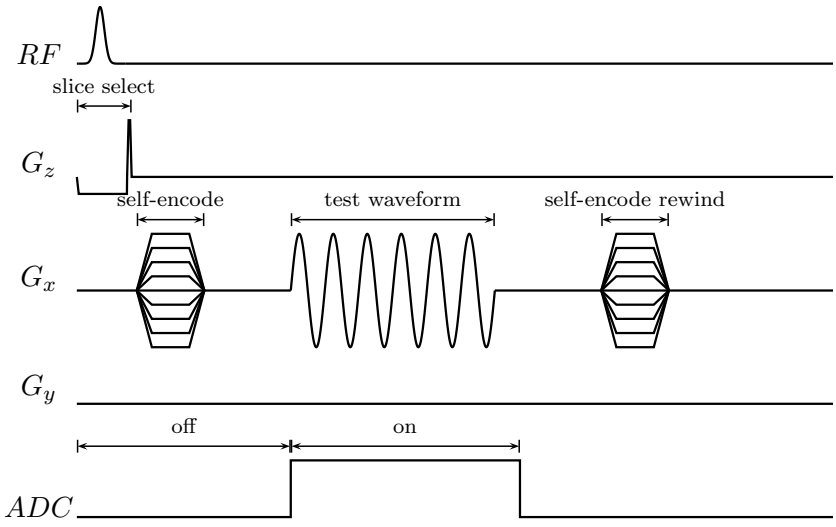

Figure 2-1: Sequence for self-encode method characterizing a test waveform gradient on the x-axis.

n can be given by the following equation:

$$k_c(n,t) = k_{se}(n) + k_c(t) \tag{2.4}$$

where (from equation 2.2)

$$k_c(t) = \frac{\gamma}{2\pi}\int_0^t G_c(\tau)d\tau. \tag{2.5}$$

Note that time t is equal to 0 at the start of $G_c(t)$. The sequence events can be summarized in figure 2-1. In this figure, a sinusoidal test waveform on the x-axis is being characterized. The signal is read when the analog to digital converter (ADC) is turned on. The self-encode loops are played before the test waveform gradient, and a rewinder is used after the test gradient to return the system back to origin in k-space, where $k_x = 0$.

Because a large phantom is excited at the isocenter, the signal has a peak when $k(n,t) = 0$. Since $k(n,t)$ and $k_{se}(n)$ are known values, the points on the test k-space trajectory can be estimated as

$$k_c(t) = k(n,t) - k_{se}(n). \tag{2.6}$$

The collected data can be placed in a two-dimensional array with time t as one axis and the self-encode number n as the other axis. For a given $t = t_0$, there is an associated array in the self-encode dimension. The data of that array contains the Fourier transform of the

excited phantom shifted from the origin by $-k_c(t_0)$. The point $-k_c(t_0)$ can be determined by finding the maximum value of the array.

To make the technique more robust and to increase the k-space resolution, a fitting algorithm is used to find a more accurate estimation of $-k_c(t_0)$. The sampled data can be fitted with a polynomial (proposed by Takahashi *et al* [8]), a Gaussian, or even a *sinc*. Knowing the ideal one-dimensional image of the given phantom allows for a better fitting.

Additionally, given a large enough value for k_{max}, the phase can be extracted from $\mathcal{FT}\{k(n,t_0)\}$, the Fourier transform of the data along the self-encode axis [1]. Since $k(n,t_0)$ is an image of the phantom shifted by $-k_c(t_0)$, the amount of shift $-k_c(t_0)$ can be extracted from the phase of $\mathcal{FT}\{k(n,t_0)\}$. The phase is a linear function whose slope is proportional to $-k_c(t_0)$.

The linear phase fitting method is much more robust and requires fewer data points compared to polynomial or Gaussian fitting. However, the method cannot be used for test waveform gradients with values of k_{max} that are too small. With a smaller k_{max}, the $\mathcal{FT}\{k(n,t_0)\}$ image has zero-crossings closer to the origin. In these cases, the phase becomes less and less accurate. For a $180mm$ outer diameter spherical phantom, I found that the test waveform gradients that can be characterized using linear phase fitting must have a k_{max} that satisfies this inequality: $k_{max} \geq 1000m^{-1}$. For my experiments, I used the linear phase fitting method for $k_{max} \geq 1000m^{-1}$ and the Gaussian peak-fitting method for $k_{max} < 1000m^{-1}$.

Time-varying distortions $b(t)$ caused by factors such as eddy currents can be measured and removed from the characterization. Using a Fourier transform technique, the time-varying distortion can be corrected with additional characterization data of an inverted test waveform gradient [1]. The solution can be seen in the following analysis. For measuring the test waveform gradient on the x-axis, these equations apply: $k_x(n,t) = k_{se}(n) + k_x(t)$ (obtained directly from equation 2.4) and $k_y(t) = 0$ (since the gradient on the y-axis is turned off). Through some manipulation, equation 2.1 can be rewritten as a function of n and t:

$$s(n,t) = \int_x m(x) e^{i[2\pi(k_{se}(n)+k_x(t))x+b(t)]} dx. \tag{2.7}$$

Applying a one-dimensional Fourier-transform along the self-encode direction of equation

2.7 yields

$$\mathcal{FT}\{s(n,t)\} = m(x)e^{i[2\pi k_x(t)x+b(t)]}. \tag{2.8}$$

The phase of equation 2.8, $\phi(x,t)$, can be extracted to be

$$\begin{aligned}\phi(x,t) &= 2\pi k_x(t)x + b(t) \\ &= 2\pi k_x(t)x + b_o(t) + b_e(t),\end{aligned} \tag{2.9}$$

where $b_o(t)$ is the odd part of $b(t)$, and $b_e(t)$ is the even part of $b(t)$. Data from objects scanned are real in the image domain, meaning that the phase function, $\phi(x,t)$, is odd with respect to x. Measuring an inverted waveform gradient yields a phase of $\phi_-(x,t) = -2\pi k_x(t)x - b_o(t) + b_r(t)$. The corrected k-space trajectory becomes

$$\begin{aligned}k(t) &= \frac{(\phi_+(x,t) - \phi_-(x,t))}{2} \\ &= 2\pi k_x(t)x + b_o(t).\end{aligned} \tag{2.10}$$

The self-encode method does not require any additional hardware or specially constructed phantoms. The algorithm can be performed using a standard setting of the scanner and with any large arbitrary phantom. Given the nature of the method, a large advantage of this technique is that the gradient coils can be pushed to their manufacture limits, at maximum slew rate and amplitude, and still have the waveform gradients be characterized. This procedure becomes quite useful when analyzing the gradient distortion that need speed and reach to extreme values of k-space.

The self-encode method presents a few drawbacks however. First, the sequence requires a long scan time and also a long reconstruction time. For a TR of $300ms$ and a resolution of 80, a scan time of $0.3s \times 80 = 24s$ is required. To correct for time-varying distortion with the inverted test waveform, the scan duration is then doubled. Added to that, in reconstruction, either the linear phase fitting or the peak fitting algorithm is performed on multiple different arrays, requiring a nontrivial amount of processing time. Second, the method assumes that the self-encode loops themselves are well-formed and accurate. Any inconsistencies with these encode loops will make the characterization inaccurate. Lastly, although the procedure can be performed with any arbitrary phantom, the reconstruction algorithm is still dependent on the size and shape of the phantom. The method requires

additional work to fine-tune the parameters for each specific phantom.

2.2.2 Slice selection method

In comparison to the self-encode method, the voxel/slice excitation method requires significantly less scan time and reconstruction time. Gradient characterization using a slice excitation was first proposed by Duyn *et al* [2]. Kim *et al* extended the slice selection method to excite voxels for spectroscopic imaging [4]. The slice selection method and the voxel excitation method are similar to the procedure proposed by Mason *et al* [5]. The main difference is that in Mason's method a small reference phantom is used; in these other methods the excitation singles out positions where the small phantom would have been.

I analyzed and tested the algorithm proposed by Duyn *et al*. In this method, a number of off-isocenter slices are excited and the k-space trajectory is extracted from the phase. To characterize the gradient, the measured gradient can be computed from the k-space trajectory.

To measure the k-space trajectory on the x-axis, a thin slice in the yz-plane is excited at a position x_0 away from isocenter. The test waveform gradient $G_x(t)$ (with a corresponding $k_x(t)$ trajectory) is then played on the x-axis (figure 2-2(a)). In the signal equation 2.1, the signal $m(x, y)$ can be approximated to an impulse on the x-axis, or $m(x, y) = \delta(x - x_0)$. Additionally, with the gradients in the y-axis turned off, the value of $k_y(t)$ is equal to 0. Equation 2.1 can be simplified to

$$\begin{aligned} s(t) &= \int_y \int_x \delta(x - x_0) e^{i[2\pi k_x(t)x + b(t)]} dx dy \\ &= C_1 e^{i[2\pi k_x(t)x_0 + b(t)]}, \end{aligned} \tag{2.11}$$

where C_1 is proportional to the slice length in y. The phase $\phi(t)$ can be extracted from $s(t)$ in equation 2.11 to be $\phi(t) = 2\pi k_x(t)x_0 + b(t)$. An unwrapping algorithm must be used to properly extract $k_x(t)$.

Data for another x-axis slice excitation at the same position x_0 is acquired, but during the read-out following this excitation, the test waveform gradient is not applied (see figure 2-2(b)). For this case, the expression $k_x = 0$ holds, and equation 2.11 becomes

$$s(t) = C_2 e^{ib(t)},$$

(a)

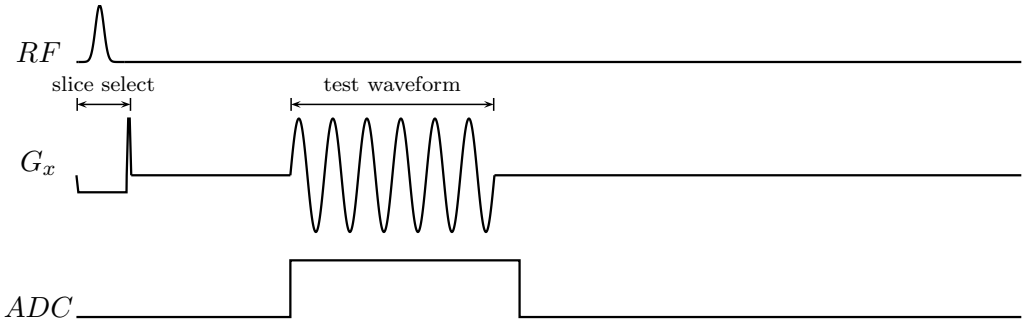

(b)

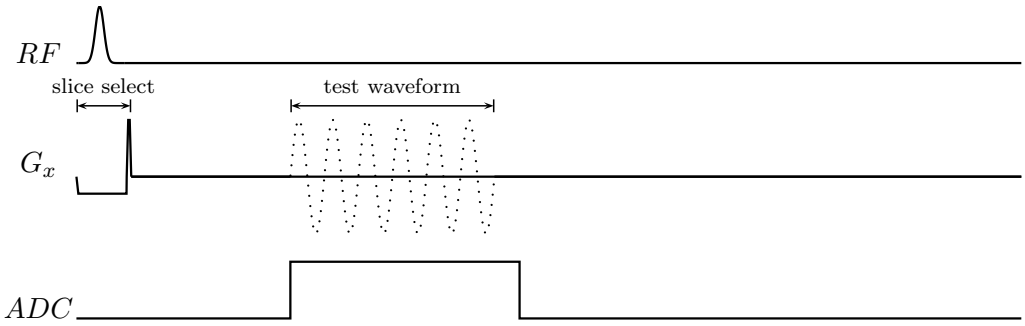

Figure 2-2: Sequence for slice selection method characterizing a test waveform gradient on the x-axis: (a) gradients *on*, (b) gradients *off*.

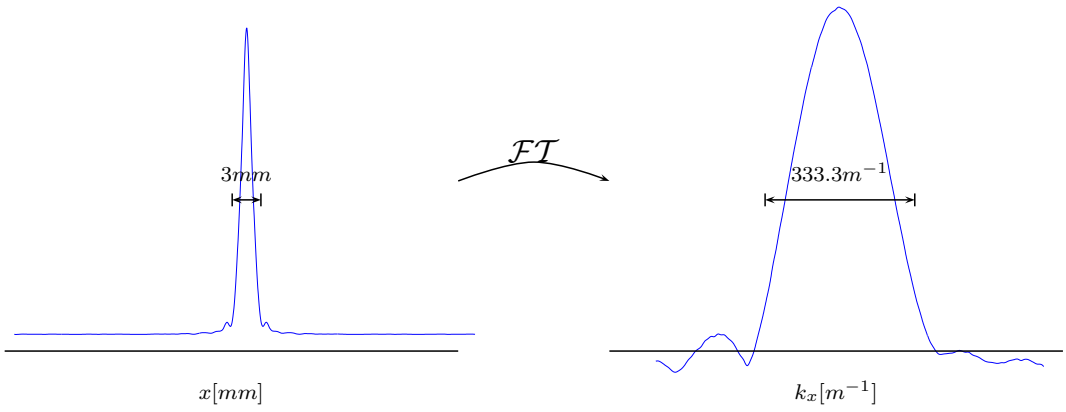

Figure 2-3: Plots of actual data on the x-axis showing the relationship between slice thickness ($\Delta_x = 3mm$) and k-space zero crossing ($2k_{zc} = 333.3m^{-1}$).

where C_2 is some scaling factor that is not important for this algorithm. During this measurement, any time-varying inhomogeneities ($b(t)$) not specific to a particular waveform gradient is measured. From the difference in phase of the two scans, the result is equal to

$$\Delta\phi(t) = 2\pi k_x(t)x_0 + \Delta b(t). \tag{2.12}$$

Note that $\Delta b(t) \neq 0$ because of time-varying distortions resulting from the test waveform gradient itself.

One set of slice excitation is enough to estimate $k_x(t)$. Since each set of scans require only two TRs, data for multiple slice locations can be obtained to reduce noise and to improve the estimation. Duyn *et al* used 3 slice locations [2]. For multiple slices, the k-space trajectory $k_x(t)$ can be extracted using linear least squares estimation (LLSE).

$$\begin{pmatrix} -\Delta\phi_0(t)- \\ -\Delta\phi_1(t)- \\ \vdots \\ -\Delta\phi_n(t)- \end{pmatrix} = 2\pi \begin{pmatrix} x_0 & 1 \\ x_1 & 1 \\ \vdots & \vdots \\ x_n & 1 \end{pmatrix} \begin{pmatrix} -k_x(t)- \\ -\Delta b(t)- \end{pmatrix}$$

$$\begin{pmatrix} -k_x(t)- \\ -\Delta b(t)- \end{pmatrix} = \frac{1}{2\pi} \begin{pmatrix} x_0 & 1 \\ x_1 & 1 \\ \vdots & \vdots \\ x_n & 1 \end{pmatrix}^{\dagger} \begin{pmatrix} -\Delta\phi_0(t)- \\ -\Delta\phi_1(t)- \\ \vdots \\ -\Delta\phi_n(t)- \end{pmatrix} \tag{2.13}$$

where $\dagger$ is the pseudo-inverse: $A^{\dagger} = (A^T A)^{-1} A^T$

In equation 2.13, the time-varying $\Delta b(t)$ is extracted and may be analyzed. This distortion term can also be left in $k_x(t)$, so the final estimated k-space trajectory will incorporate all the different distortion effects. In this case, equation 2.13 simplifies to

$$\begin{pmatrix} -k_x(t)- \end{pmatrix} = \frac{1}{2\pi} \begin{pmatrix} x_0 \\ x_1 \\ \vdots \\ x_n \end{pmatrix}^{\dagger} \begin{pmatrix} -\Delta\phi_0(t)- \\ -\Delta\phi_1(t)- \\ \vdots \\ -\Delta\phi_n(t)- \end{pmatrix} \tag{2.14}$$

The same algorithm described can be used to characterize trajectories in the y-axis and

the z-axis. The only difference is that the slice selection and test waveform gradients are played on a different axis.

The slice selection is assumed to be an approximate impulse $\delta(x)$; however, this is not the case in practice. The "impulse" has a finite width determined by the slice thickness Δ_x. The Fourier-transform of this "impulse" is equal to $\frac{sin(\pi k_x \Delta_x)}{\pi k_x}$, a $sinc$ function with its first zero crossings, k_{zc}, at

$$|k_{zc}| = \frac{1}{\Delta_x}. \tag{2.15}$$

Therefore, the k-space trajectories to be characterized must have a maximum k-space value, k_{max}, that is absolutely smaller than k_{zc} from equation 2.15. The value of k_{max} must equal the value of k_{zc} because the amplitude is negligible at k-space locations close to the zero crossings. Overall, the larger the value of Δ_x, the larger the value of k_{max} possible for the test k-space trajectory. The value of Δ_x cannot be decreased indefinitely because of its proportional effect on the signal to noise ratio (SNR). Duyn *et al* used a slice thickness Δ_x equal to $3mm$ [2], yielding a maximum k_{max} of $333.3m^{-1}$ as seen in figure 2-3. In practice, k_{max} should be limited to be less than 90% of k_{zc} ($k_{max} < 300m^{-1}$ for $\Delta_x = 3mm$) to safely avoid the amplified noise near k_{zc}.

Another nontrivial detail to this technique is that there is a minimum sampling rate f_s required for the ADC readout to allow for proper phase unwrapping. Between each sample, I set the maximum phase difference to be less than 2π. Under this criteria, the phase algorithm consists of setting the phase difference between each sample to be at a minimum. Using equation 2.12 and considering $\Delta b(t)$ as part of $k_x(t)$, this condition can be generalized through the following derivation:

$$\begin{aligned} \Delta\phi(t_1) - \Delta\phi(t_0) &\leq 2\pi \\ 2\pi(k_x(t_1) - k_x(t_0)) &\leq 2\pi \\ k_x(t_1) - k_x(t_0) &\leq 1 \\ f_s \geq \frac{dk_x(t)}{dt} &= \frac{\gamma}{2\pi} G_x(t) \end{aligned} \tag{2.16}$$

From equation 2.16, the sampling rate, f_s, must be greater than the maximum value of $\frac{\gamma}{2\pi} G_x(t)$.

In summary, the slice selection method does not require any unique hardware setup. This

is an advantage shared by the self-encode method. The algorithm can be implemented with trivial modifications to a given pulse sequence and can be used on any arbitrary phantom. Additionally, this method has a much shorter scan time and reconstruction time compared to the self-encode method. For $TR = 300ms$ and 3 different slice locations, a scan time of $0.3s \times 3 = 0.9s$ is needed. For an additional $b(t)$ measurement, the total scan duration becomes $1.8s$. A time duration of $1.8s$ is a vast improvement over the $24s$ duration required by the self-encode method. Also, unlike the self-encode method, detailed knowledge about the phantom scanned is unnecessary. However, this procedure has its own disadvantages. Given equation 2.15, the slice selection method cannot characterize waveform gradients that traverse too far in k-space. There is also a design trade-off between SNR and the maximum possible k-space value k_{max}.

2.2.3 Self-encoded slice selection method

The self-encode method described in section 2.2.1 and the slice selection method described in section 2.2.2 has its own advantages and disadvantages. The self-encode method allows for test waveform gradients that push to the MR system's maximum gradient amplitude and maximum slew rate. However, this method has the cost of a large time duration for data acquisition and reconstruction. The slice selection method backs away from the system's limits, but it allows for a much faster algorithm. I propose combining the two methods into the self-encoded slice selection method to utilize both algorithms' advantages.

The proposed method is a derivation of the slice selection method. But, the algorithm requires a minor modification if the maximum k-space value of the test waveform gradient, k_{max}, is greater than the first zero crossing, k_{zc} (described by equation 2.15). As described by the previous section (section 2.2.1), a safe k_{max} is where $k_{max} < 0.9k_{zc}$ or $k_{max} < 0.9\frac{1}{\Delta_x}$ for a slice thickness of Δ_x. For trajectories with $k_{max} > 0.9k_{zc}$, only portions of the test waveform trajectories that have k-space values within 90% of k_{zc} can be properly characterized. In figure 2-5, 90% of k_{zc} is denoted by the light gray box. For the x-axis, this characterizable region R_c is defined to be

$$R_c = \{k_x : -0.9k_{zc} < k_x < 0.9k_{zc}\}, \tag{2.17}$$

where k_{zc} is defined by equation 2.15.

(a)

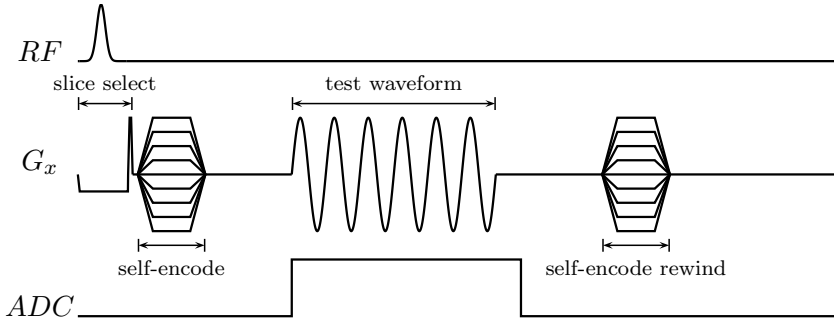

(b)

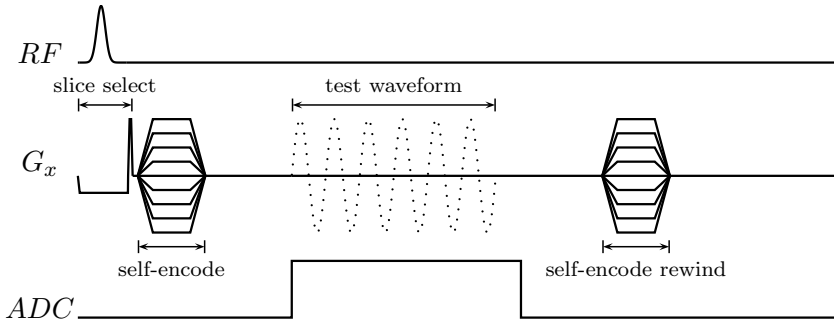

Figure 2-4: Sequence for self-encoded slice selection method characterizing a test waveform gradient on the x-axis: (a) gradients *on*, (b) gradients *off*.

(a)

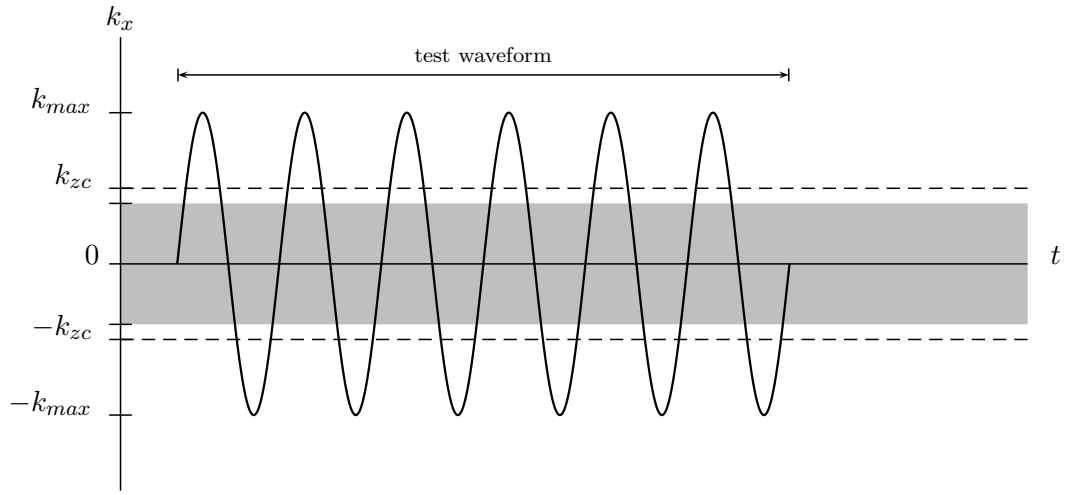

(b)

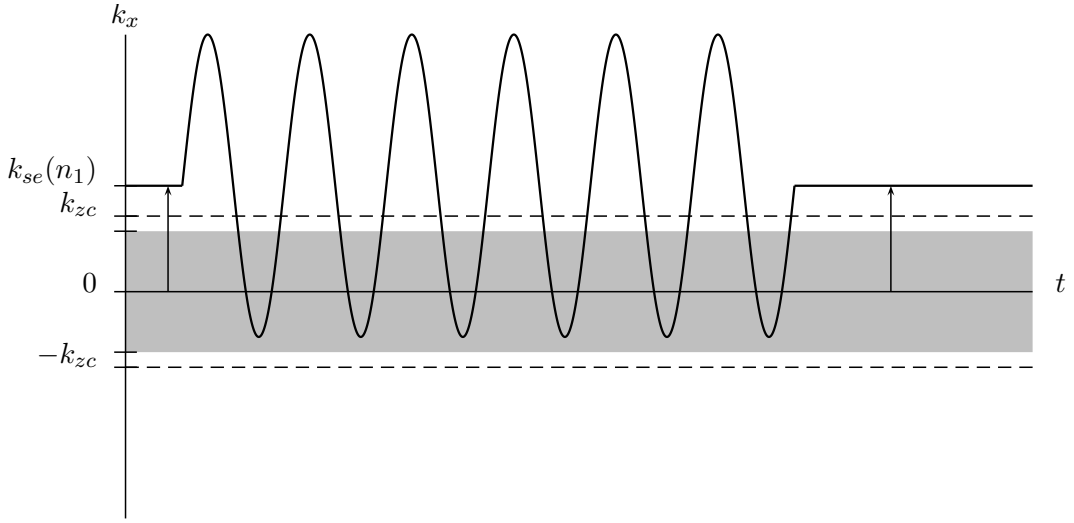

Figure 2-5: Diagram of the self-encoded slice selection method: (a) $k_{se}(n_0) = 0$, (b) a shift in k_x as a result of $k_{se}(n_1) > 0$

In order to characterize test waveforms that have $k_{max} > 0.9k_{zc}$, self-encode loops are played before the test waveform gradient (as shown in figure 2-4). These self-encode loops shift the test waveform trajectory by $k_{se}(n)$ such that a different portion of the k-space trajectory is within R_c.

The number of self-encode loops, N_{se}, depends on the range of R_c and the value of k_{max}. In the self-encoded slice selection method, the equation for N_{se} becomes

$$N_{se} = \left\lceil \frac{k_{max}}{0.9k_{zc}} \right\rceil . \tag{2.18}$$

A modification to equation 2.3 of the self-encode method, the k-space shift $k_{se}(n)$ of the n-th self-encode is defined to be

$$k_{se}(n) = \begin{cases} 0, & \text{for } N_{se} = 1 \\ k_{max} - \frac{k_{zc}}{2} - n\left(\frac{2k_{max}}{N_{se}}\right), & \text{for } N_{se} > 1 \end{cases}, \qquad \text{where } n = 0, 1, 2, \ldots N_{se} - 1. \tag{2.19}$$

To avoid using more self-encode loops than necessary, a separate self-encode gradient can be used to center the k-space trajectory. With this addition, the test waveform gradient may have a smaller k_{max}. If this approach is used, care must be taken during data processing in shifting the trajectory back to its original position.

Extracting the measured k-space trajectory is similar to the procedure described for the slice selection method in section 2.2.2, and it is exactly the same if $N_{se} = 1$. Additionally, the self-encoded slice selection method uses the same approach of reducing the time-varying $b(t)$ effect (described by equation 2.12) and the same approach of extracting the final k-space trajectory with LLSE (shown in equation 2.14).The same criteria for the sampling rate f_s (defined by equation 2.16) also still applies. Modification to characterize test waveform gradients on the y-axis or z-axis is the same. The only difference from the previous method is that during data processing the k-space trajectory must be spliced together.

The test waveform trajectory is characterized in different pieces that are determined by R_c. To characterize the entire k-space trajectory, the N_{se} number of pieces must be spliced together. The phase $\phi(n, t)$ for each of the pieces does not align properly because of the additional phase induced by the self-encode loops and some time-varying distortions. To overcome this obstacle, a 0.6 factor is used instead of the 0.9 factor in equation 2.18. This

guarantees an overlap between each consecutive piece. Equation 2.18 is redefined to be

$$N_{se} = \left\lceil \frac{k_{max}}{\mathbf{0.6}k_{zc}} \right\rceil . \tag{2.20}$$

At each overlapping region, the average distance between each consecutive segment is used to shift and connect the following piece of k-space trajectory with the preceding piece. In this way, the entire k-space trajectory is spliced together. Afterward, the measured k-space trajectory may need to be re-centered. A different factor other than 0.6 in equation 2.20 can be used; the only criteria for this factor is that it must be less than 0.9. Note that, with a smaller factor, the overlapping region between each piece is larger resulting in a more accurate splicing.

There are a couple of trade-offs particular to this method. One trade-off is between N_{se} and the accuracy of the splice algorithm. Decreasing the 0.9 factor in equation 2.18 yields more accurate splicing but a longer scan time due to a larger N_{se}. Another design parameter, the slice thickness (Δ_x), addresses the trade-off between SNR and N_{se}. A decrease in Δ_x results in lower SNR but a shorter scan time due to a smaller N_{se} (according to equation 2.15 and equation 2.18)).

One assumption made in this algorithm is that the self-encode loops (seen in figure 2-4) are well formed and accurate. The same assumption is made in the self-encode method. However, the self-encode loops can be verified and corrected through the gradient characterization of the self-encode loops themselves. In this way, the accuracy of the self-encode loops can be confirmed or improved.

In short, the self-encoded slice selection method uses the slice selection method's speed and at the same time uses the self-encode method's ability to characterize at the system's limits. The proposed self encoded slice selection method provides for an improved alternative to measure and correct k-space trajectories.

As noted before, the self-encode method with $N_{se} = 80$ requires a scan time of approximately $24s$ to measure 1 waveform with $TR = 300ms$. The method requires $48s$ for characterization and correction of any time-varying waveform-independent distortions. With the self-encoded slice selection method, a lower N_{se} (typically with a value in the range 1–5 for normal waveform gradients) is needed to produce the same characterization quality. Even with $N_{se} = 4$ and the same TR, the same waveform gradient analysis will require a scan

time of only 7.2s for 3 slice locations and $b(t)$ elimination. The reconstruction time for the self-encoded slice selection method is also much shorter than for the self-encode method. The difference becomes even more noticeable when multiple test waveform gradients are being characterized.

2.3 Gradient transfer function

Characterizing each gradient desired on the scanner can be costly in terms of time. Kerr proposed a method for characterizing the gradient system as a linear time-invariant transfer function $H(f)$ in his PhD thesis [3]. With a good model of $H(f)$, the actual gradient trajectory can be predicted quite well given the waveform gradient inputted into the system. Distortion correction can be accomplished before the gradients are even played. Calculation of the transfer function $H(f)$ can be performed once per scanner and used multiple times for accuracy improvement in data acquisition or data post-processing. Due to linearity, $H(f)$ can be applied to both the waveform gradients or the waveform k-space trajectories.

2.3.1 Frequency-domain approach

In his thesis [3], Kerr proposed characterizing sine waves of different frequencies as a method of measuring the gradient system transfer function. To characterize the sinusoid waves, he uses the self-encode method (section 2.2.1). With this approach, the gradient amplitude and slew rate can be pushed to the system's limits to allow for a more general transfer function. However, if sinusoid waves with 76 different frequencies are measured using the self-encode method of 80 resolution and a TR of 300ms, the characterization of the system would take approximately 20min to also incorporate waveform-independent distortion corrections. Additionally, multiple experiments might be also performed to test the reproducibility of the modeled transfer function. Fortunately, the scan time can be greatly reduced if the proposed self-encoded slice selection method (section 2.2.3) is used. Given an average number of self encode loops in this method to be 5 with 3 different slice locations, the entire experiment time is reduced by a factor of 4.

Depending on the allotted time determined by TE, one to three periods of the test sinusoid wave gradient is played before data is obtained for characterization (see figure 2-6). The extra periods give the system ample time for a sinusoidal steady state response [3].

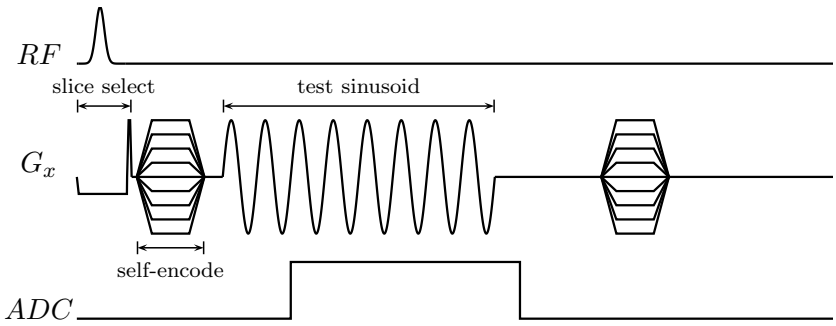

Figure 2-6: Sequence for gradient transfer function characterization on the x-axis using the self-encoded slice excitation algorithm. This sequence is when the gradient test waveforms are turned *on*.

Assuming linear time-invariance, the gradient system is defined as:

$$G(t, f_0) = A(f_0)sin(2\pi f_0 t) \longrightarrow \begin{bmatrix}\text{Gradient} \\ \text{System}\end{bmatrix} \longrightarrow \bar{G}(t, f_0) = |H(f_0)|A(f_0)sin(2\pi f_0 t + \angle H(f_0)) \tag{2.21}$$

where $G(t, f_0)$ is the test sinusoidal wave gradient with a frequency of f_0, and $\bar{G}(t, f_0)$ is the output from the gradient system. The function $\bar{G}(t, f_0)$ can be obtained by applying a characterization algorithm, such as the self-encode method. The variable $A(f_0)$ is the amplitude of the sinusoid such that either the maximum gradient amplitude or maximum slew rate is reached. From equation 2.21, the magnitude and phase of $H(f)$ can be readily extracted from $\bar{G}(t, f_0)$.

To minimize error, the frequencies (f) are chosen such that the periods are multiples of the gradient raster time (t_{gr}), the time that it takes the gradient system to change from one gradient value to the next. Under this criteria, $G(t, f)$ is assumed to be well-formed. Additionally with this limitation, only a finite number of frequencies can be characterized, where

$$f = \frac{1}{kt_{gr}} \qquad \text{where } k = 1, 2, 3, \ldots \tag{2.22}$$

The maximum frequency f possible is limited by t_{gr}.

Figure 2-7 shows an example self-encoded slice selection characterization of a sinusoid waveform gradient with $f = 1111.11Hz$. The differences between the output sinusoid waveform and the input sinusoid waveform are very small as expected. These small differences,

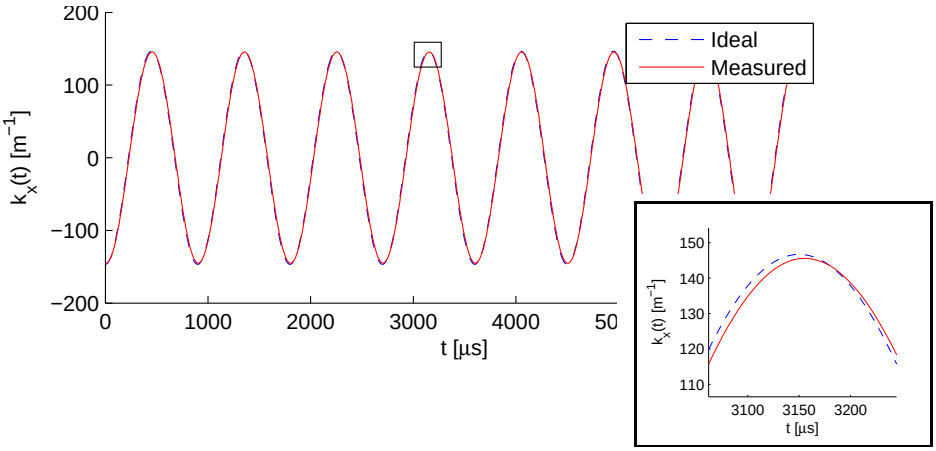

Figure 2-7: Graph of ideal (*blue dashed*) and measured (*red solid*) sine wave with $f = 1111.11Hz$. Characterized on the x-axis using the self-encoded slice selection method.

however, are what characterizes $H(f)$. From the magnified plot in figure 2-7, the amplitude decrease (corresponding to $|H(1111.11Hz)|$) and the phase shift (corresponding to $\angle H(1111.11Hz)$) can be seen.

Using the frequencies specified by equation 2.22, samples of the gradient transfer function $H(f)$ can be measured. Kerr proposed fitting these data points of $|H(f)|$ and $\angle H(f)$ separately with spline interpolation. At the DC point and at higher frequencies, he used a linear extrapolation of the three closest measured points to estimate the transfer function at these two extremities [3]. According to equation 2.22, samples at higher frequencies naturally have larger and larger spacing between each point. This property makes the modeled transfer function more inaccurate at these higher frequencies.

2.3.2 Time-domain approach

Another approach in measuring $H(f)$ is through the characterization of time-domain input responses. Modifying equation 2.21 produces the following generalization:

$$x(t) \longrightarrow \begin{bmatrix} \text{Gradient} \\ \text{System} \end{bmatrix} \longrightarrow y(t) \tag{2.23}$$

where $x(t)$ is the input test gradient and $y(t)$ is the output gradient measured through one of the gradient characterization methods, such as the self-encode method or the self-encoded slice selection method. Given an arbitrary input $x(t)$, the gradient system transfer function

$H(f)$ can be approximated to be

$$H(f) = \frac{X(f)}{Y(f)}, \tag{2.24}$$

where $X(f) = \mathcal{FT}\{x(t)\}$ and $Y(f) = \mathcal{FT}\{y(t)\}$.

Ideally, if $x(t) = \delta(t)$, the output would be the time-domain impulse response $h(t)$, the inverse Fourier-transform of $H(f)$. Unfortunately, the $\delta(t)$ function with infinite height and infinitesimally small width is impossible to implement in practice. An important design consideration is the actual shape of $X(f)$. The input, $x(t)$, can be set to a step function, $u(t)$, or a ramp function, $tu(t)$. With $x(t) = u(t)$, the Fourier transform is equal to $X(f) = \frac{1}{i2\pi f} + \frac{1}{2}\delta(f)$. And, with $x(t) = tu(t)$, the Fourier transform is equal to $X(f) = i\frac{1}{2\pi}\frac{d}{df}\left(\frac{1}{i2\pi f} + \frac{1}{2}\delta(f)\right)$. The singularities $\delta(f)$ and $\frac{d}{df}\delta(f)$ present an obstacle when computing $H(f)$. In practice, these singularities appear as very narrow *sinc*'s that reduce the zero crossing of $X(f)$. These *sinc* functions are present because the measured data has a finite duration that is on the order of μs's. The low zero crossings limit the approximation of $H(f)$ because $H(f)$ can only be calculated for frequencies smaller than the first zero crossings of $X(f)$. Close to the zero crossings of $X(f)$ the negligible amplitude is overpowered by noise.

One possible approach for the time-domain approach is the use of $x(t) = u(t)$ and characterizing its derivative, an impulse $\delta(t)$, rather than the step function itself. By setting the gradient input to $u(t)$, the k-space trajectory measured is a ramp. To analyze $\frac{dx}{dt}(t)$, two derivatives are required, and these derivatives introduce too much noise to properly compute $H(f)$.

With this design consideration, the $x(t)$ I propose for the time-domain approach is a very narrow triangle input with its slope determined by the maximum slew rate, m_{sr} ($[T/m/s]$), and its peak determined by the maximum gradient amplitude, g_{max} ($[T/m]$).

$$x(t) = \begin{cases} m_{sr}t, & \text{for } 0 \leq t \leq \frac{g_{max}}{m_{sr}} \\ g_{max} - m_{sr}(t - \frac{g_{max}}{m_{sr}}), & \text{for } \frac{g_{max}}{m_{sr}} < t \leq 2\frac{g_{max}}{m_{sr}} \\ 0, & \text{for } 2\frac{g_{max}}{m_{sr}} \leq t \end{cases}. \tag{2.25}$$

Equation 2.25 demonstrates a triangle waveform gradient input that pushes the system's limits, allowing for a more general approximation of $H(f)$ with higher possible values of f. Given $x(t)$ in equation 2.25, the magnitude of the Fourier transform of $x(t)$ is described by

the following expression:

$$|X(f)| \propto \left(\frac{sin(\pi \frac{g_{max}}{m_{sr}} f)}{\pi \frac{g_{max}}{m_{sr}} f} \right)^2 . \tag{2.26}$$

From equation 2.26, the first zero crossing, f_{zc}, of $H(f)$ is when

$$|f_{zc}| = \frac{m_{sr}}{g_{max}}. \tag{2.27}$$

To characterize $H(f)$ with the highest possible frequencies, g_{max} should be minimized and m_{sr} should be maximized, taking care to keep these variables within the system's limits. The trade-off with input $x(t)$ from equation 2.25 is between a larger characterizable region of $H(f)$ and better SNR. The characterizable region is determined by f_{zc}, and SNR is influenced by g_{max}.

Another point of consideration is that the gradient raster time, the period of $x(t)$, may be greater than the ADC sampling period, the period of $y(t)$. To overcome this problem when calculating $H(f)$, a linear interpolation approximation is used to set the period between each sample of $x(t)$ equal to the period between each sample of $y(t)$.

The time-domain characterization of the gradient transfer function is prone to noise because a smaller data set is used. However, the noise can be minimized by taking the average of multiple experiments. To eliminate high frequency noise, low pass filtering can also be used on the data set before $H(f)$ calculation. Overall, this method provides a quicker way of calculating $H(f)$ with a higher resolution in regards to f. Additionally, the transfer function, $H(f)$, measured using the time-domain analysis can be verified using the frequency-domain algorithm described in section 2.3.1.

Chapter 3

Experiment

The different gradient characterization methods were first analyzed and tested. After the methods yielded consistent results, they were used to compute the gradient system transfer function, $H(f)$. Section 3.1 describes the material and apparatus used for experimentation. Section 3.2 describes the results of characterizing $H(f)$ using the frequency-domain approach, and section 3.3 does the same for the time-domain approach.

3.1 Material/Apparatus

The measurements were acquired on the 3T Siemens Tim Trio $60cm$ full-body magnetic resonance scanner (Erlangen, Germany). The MR scanner has an absolute maximum gradient amplitude of $40mT/m$ and an absolute maximum slew rate of $170.004T/m/s$. A spherical phantom filled with $1.25g$ $NiSO_4 \cdot 4H_2O$ per $1000g$ of H_2O was used for all the experiments. The head phantom has an outer diameter of $180mm$ and an inner diameter of $170mm$. Data obtained was processed offline using Matlab, version 7.2 (The MathWorks, Inc., Natick, MA, USA).

A TE of $16ms$ and a TR of $300ms$ were used for each scan. Spoilers, waveform gradients that shift any residue energy away from the point of interest, and rewinders, waveform gradients that return the k-space trajectory back to the origin, were used to allow for a faster acquisition time. The sampling rate, f_s, was held constant at $200Hz$, yielding a sampling period of $5\mu s$.

3.2 Frequency-domain approach

The bulk of the analysis was done using the frequency-domain approach. In section 3.2.1, description is provided for how the algorithm was set up. Next, in section 3.2.2, the results of the frequency-domain approach are described.

3.2.1 Setup

In order to estimate the gradient system transfer function $H(f)$, 76 different locations of $H(f)$ where sampled using frequencies f logarithmically spaced apart in the range of $150Hz$–$6000Hz$. According to equation 2.22, obtaining data for more than 76 frequencies in the range of $150Hz$–$6000Hz$ would only oversample the lower frequencies. These samples of $H(f)$ were obtained through the characterization of sinusoid gradients with appropriate frequencies. The sinusoid gradients were first measured in increasing frequency order, and then they were measured in decreasing frequency order. This experiment tested to see if the characterization of the sinusoid gradients were affected by the order that it was measured. Fortunately, no differences were found in the characterization of $H(f)$ when the measurement order was altered.

In order to characterize $H(f)$ at the system's limits, the sinusoid waveform gradients were set at maximum amplitude when permitted. Otherwise, the sinusoid waveforms were set to a gradient amplitude limited by the maximum slew rate. To ensure that the test waveforms were still playable on the Siemens MR scanner, the maximum gradient amplitude was slightly lower to $38mT/m$, and the maximum slew rate was slightly lowered to $160T/m/s$. Additionally, because of an increased sensitivity to the stimulation monitor on the y-axis, the maximum gradient amplitude on the y-axis was limited to $28mT/m$. Fortunately, the difference in maximum gradient amplitude used did not seem to have any effect on the results. Figure 3.2.1(a) describes the gradient amplitude used for the different frequencies ($A(f)$ from equation 2.21). Also in the figure, the maximum k-space that the sinusoid waveform reached (figure 3.2.1(b)) and the number of cycles used to characterize a specific frequency (figure 3.2.1(c)) are plotted against the corresponding frequency. The number of cycles characterized was determined by the duration of the readout, which was equal to the length of the sinusoid with the longest period. The larger number of cycles for higher frequencies was necessary because at higher frequencies, a smaller number of samples

(a)

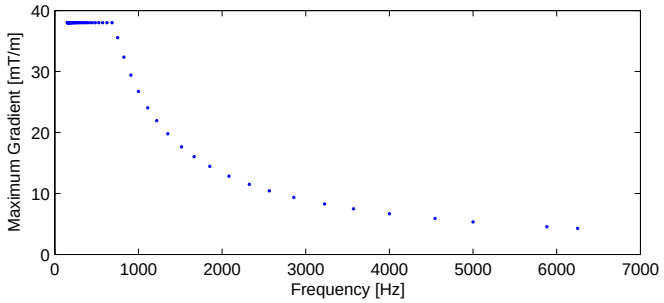

(b)

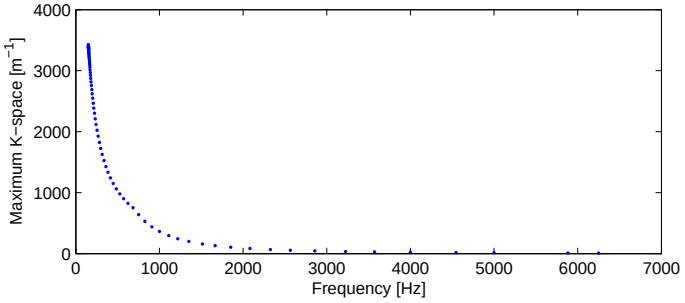

(c)

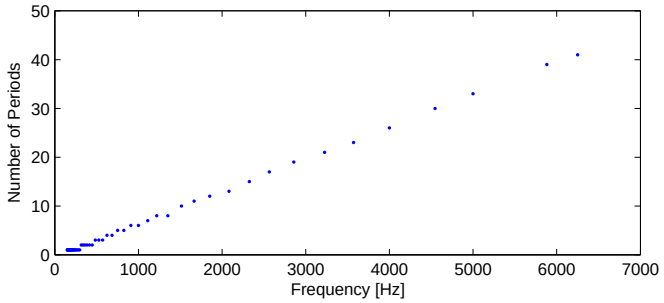

Figure 3-1: Properties of each of the sinusoid wave gradients used for estimating the gradient system transfer function $H(f)$: (a) maximum gradient amplitude, (b) maximum k-space value that the trajectory reached, (c) number of periods acquired and used for characterization.

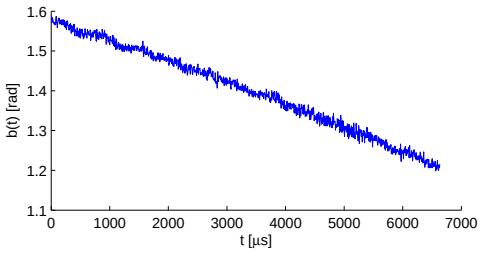

Figure 3-2: Time-varying inhomogeneities, $b(t)$, for a $3mm$ slice excite located $50mm$ off isocenter on the z-axis.

per period can be acquired.

The self-encode algorithm for gradient characterization was used to find $H(f)$. The number of self-encodes N_{se} was set to 80. Originally, the scaling factor P_{se} was set to 1.10. However, due to time-varying inhomogeneities, the measured trajectories were drifting beyond the reaches of the algorithm determined by the design parameters, beyond $k_{max}P_{se}$. So, a P_{se} value of 1.20 was used to provide sufficient k-space range. When applying both the normal waveform gradient and the inverted waveform gradient to remove any time-varying distortions (equation 2.10), the self-encode approach of estimating $H(f)$ required a scan time of 20:16min.

Next, the self-encoded slice selection algorithm was used to find $H(f)$. With this algorithm, the slice thickness Δ_x was set to $3mm$, yielding an average N_{se} of 5.4. Three different slices were used where the locations were $35mm$ to $55mm$ off isocenter. With two scans (one with the test waveform gradients off and another on) at each of the three slice locations, a total scan time of 5:36min was required to characterize $H(f)$. Since the self-encoded slice selection algorithm resulted in the same estimation of $H(f)$ as the self-encode algorithm, I will focus on the results of $H(f)$ using the self-encoded slice selection algorithm.

The time-varying inhomogeneity $b(t)$ was measured to be a linear phase drift on the order of $-10rad/s$. The linear drift had a slope independent of the scan duration but dependent on the axis, slice location, and slice thickness. Figure 3-2 shows an example of a plot of $b(t)$ for a $3mm$ slice excite on the z-axis. For long scan times the frequency-independent drift was very noticeable, so it was removed from the analysis of estimating $H(f)$.

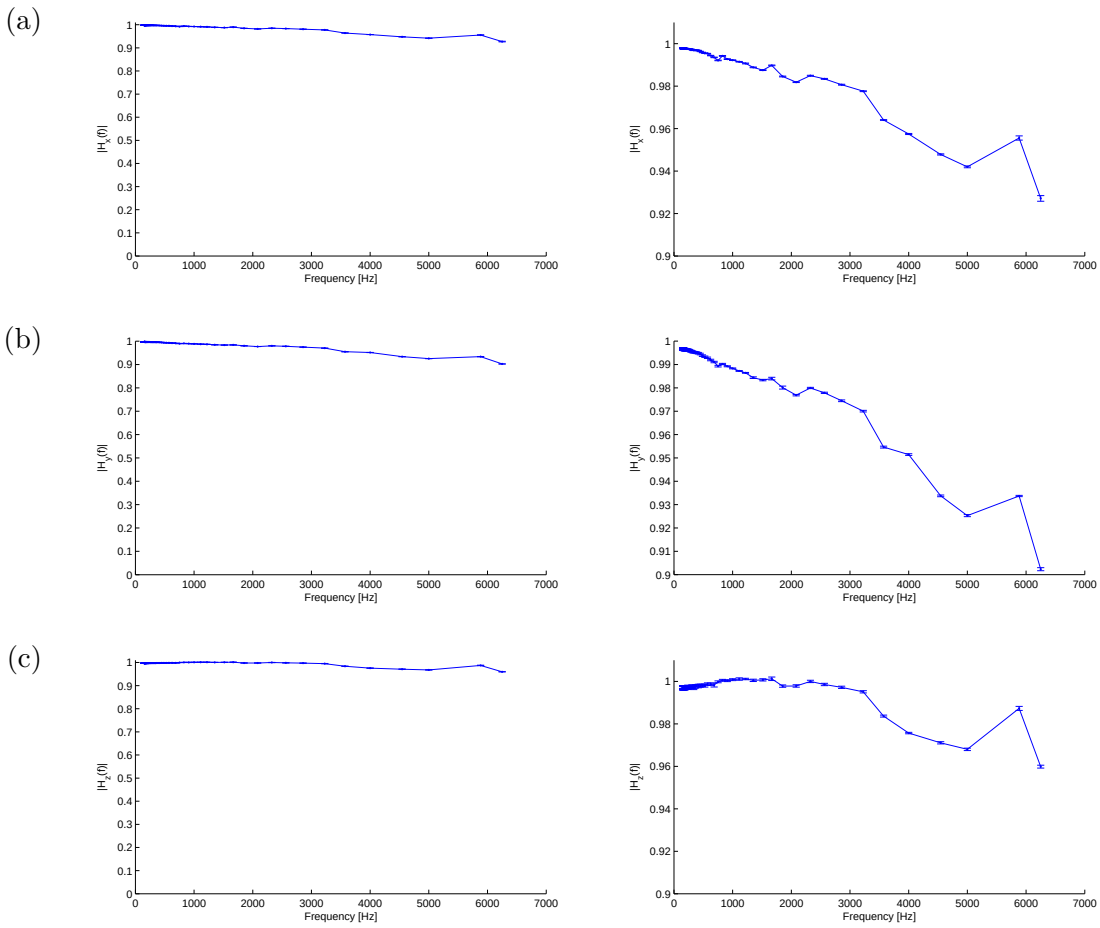

Figure 3-3: Magnitude plots of the gradient system transfer function $H(f)$ computed from a frequency-domain analysis with the self-encoded slice selection algorithm: (a) x-axis, (b) y-axis, (c) z-axis: (*left*) normal view of the magnitude plots, (*right*) a closer look at the magnitude plots with error-bars at each sample.

3.2.2 Results

Using the setup described in section 3.2.1, the gradient systems on the x-axis, y-axis, and z-axis were all characterized with respective transfer functions $H_x(f)$, $H_y(f)$, and $H_z(f)$. The self-encoded slice selection algorithm was used for each sinusoid gradient characterization. Five measurements per axis were obtained, resulting in a total of 15 different measurements. A separate transfer function was computed for each measurement. For every axis, the resulting transfer function samples were averaged to produce the final functions shown in figure 3-3 in terms of magnitude and in figure 3-4 in terms of phase. The magnitude and phase were averaged separately. The error for the computed final $H(f)$ was very small, but got larger as the frequency increased.

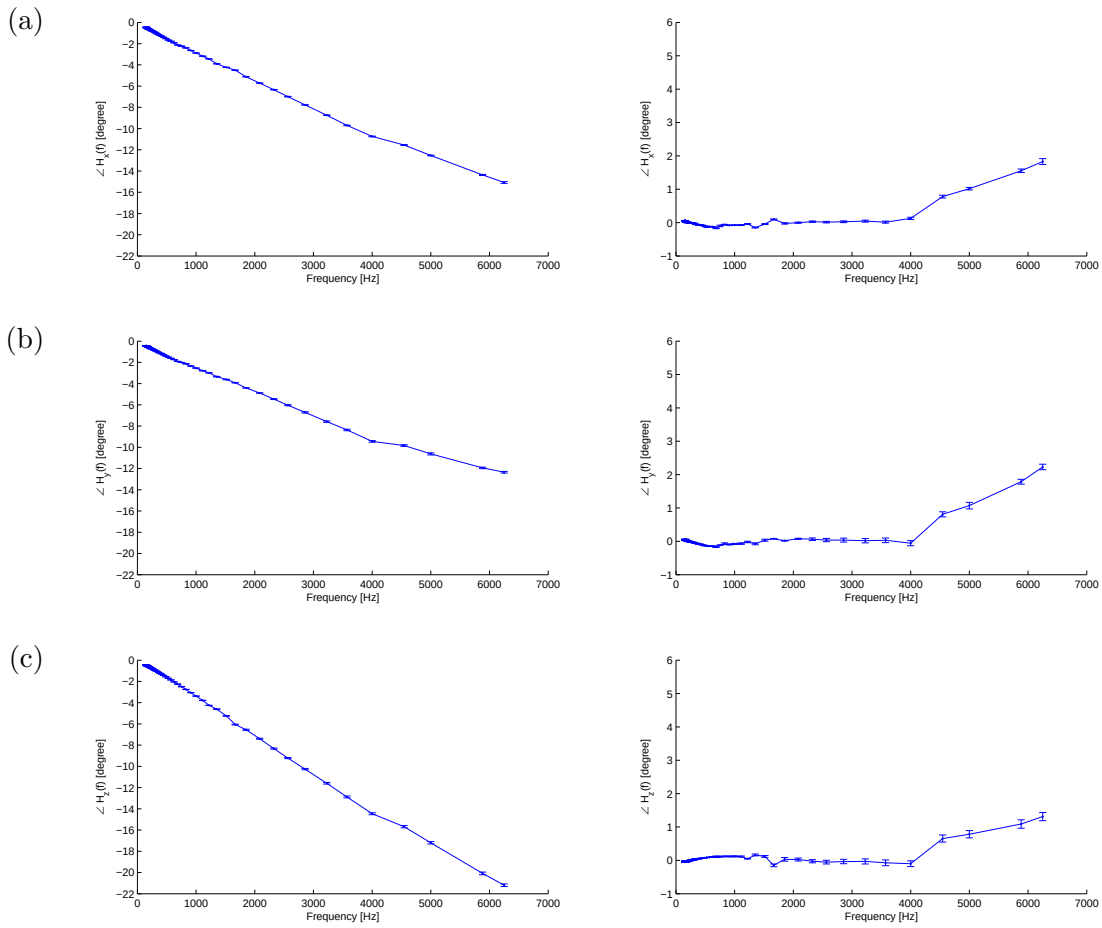

Figure 3-4: Phase plots of the gradient system transfer function $H(f)$ computed from a frequency-domain analysis with the self-encoded slice selection algorithm: (a) x-axis, (b) y-axis, (c) z-axis: (*left*) normal view of the phase plots, (*right*) phase plots with error-bars on each sample with the linear phase term removed.

At first glance, the plots in figure 3-3 and figure 3-4 show very little magnitude decay but demonstrate a linear phase shift. On closer inspection at the magnitude plot of $H(f)$, there is a slight local maximum around $6000Hz$. The cause of this deviation is yet unknown, and further experimentation is required for the explanation. However, the results are as expected; the overall trend in $|H(f)|$ is a decrease in magnitude for higher frequencies.

The linear phase shift is interpreted as a time-delay on the order of $10\mu s$. The values of the shift in each axis is summarized in table 3.1. This time-delay is not unexpected because it takes the system some time before reaching the desired gradient amplitude. By removing the linear phase term from the picture, as seen on the right-side plots of figure 3-4, the additional phase effects are more noticeable especially at higher frequencies. At

axis	linear phase $[rad/s]$	time delay $[\mu s]$
x	-4.689×10^{-5}	-7.462
y	-4.028×10^{-5}	-6.411
z	-6.318×10^{-5}	-10.055

Table 3.1: Linear phase component of $\angle H(f)$.

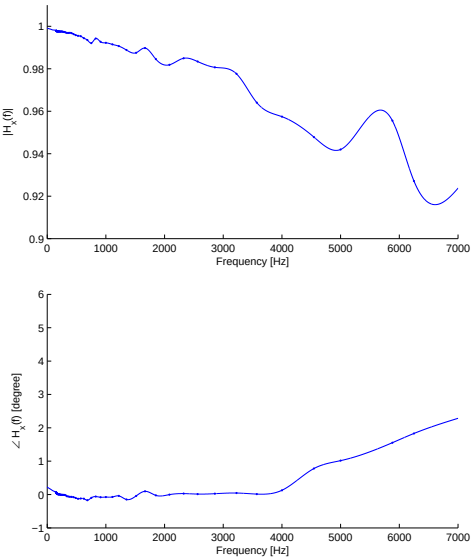

Figure 3-5: Gradient system transfer function $H_x(f)$ on the x-axis fitted using spline interpolation: (*top*) magnitude, (*bottom*) phase.

these higher frequencies, the group delay is smaller compared to the group delay at lower frequencies. I hypothesize that this discrepancy is due to the fact that at higher frequencies, the inhomogeneities become more present in the magnitude rather than in the phase. At these higher frequencies, it is harder for the gradient system to reach the specified gradient amplitudes but easier to reach the desired period.

To be able to apply these results, the gradient system transfer function $H(f)$ was fitted using linear extrapolation and spline interpolation in a method described in section 2.3.1. The $H_x(f)$ used in practice is shown in figure 3-5.

3.3 Time-domain approach

The transfer function was also found using the time-domain approach. Originally, a box function gradient input was used to approximate a step, but there was too much noise when

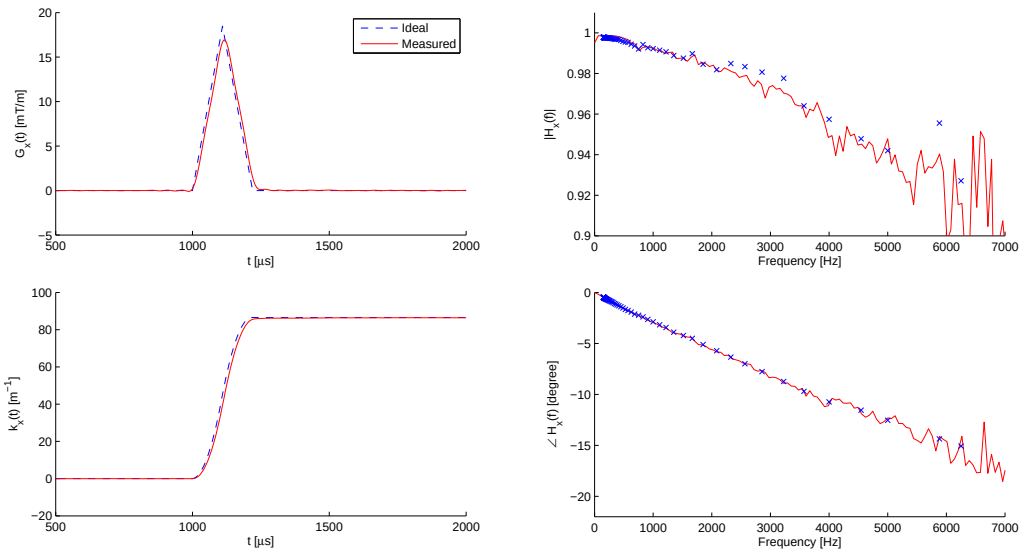

Figure 3-6: Impulse response approximated using a triangle (with a gradient peak of $20mT/m$) input on the x-axis (*clockwise from the top left*): ideal triangle $G_x(t)$ input (*blue* x) plotted with the measured output (*red solid*), $|H_x(f)|$ computed using frequency-domain analysis (*blue dashed*) compared with $|H_x(f)|$ computed using the impulse response (*red solid*), $k_x(t)$ comparison, $\angle H_x(f)$ comparison.

extracting $H(f)$. Therefore, the results presented here analyze the response to triangle gradient inputs.

The slope of these triangles was held constant at $168T/m/s$, which is a little bit less than the absolute maximum slew rate. Two different peak value of these triangle inputs were tested: $20mT/mT$ and $24mT/m$. Figure 3-6 shows the results of playing a $20mT/m$ peak triangle waveform gradient on the x-axis. The k-space trajectory was measured using the self-encoded slice selection algorithm. To compute $H_x(f)$, the ideal $G_x(t)$ was compared with the measured $G_x(t)$.

The obtained results as shown in figure 3-6 are remarkably similar to the results when $H_x(f)$ was computed using the frequency approach, figure 3-3(a) and figure 3-4(a). Comparing the frequency-domain approach and the time-domain approach, the phase and magnitude have a negligible difference for low frequencies. However, at higher frequencies the time-domain approach exhibits a lot more noise. The noise is expected due to the sensitivity of the measured output to high frequency noise. Calculated from equation 2.27, the predicted maximum characterizable frequency for $H(f)$ is less than $5750Hz$ for $24mT/m$, and $8400Hz$ for $24mT/m$. When the frequencies are close to these maximum values, the ampli-

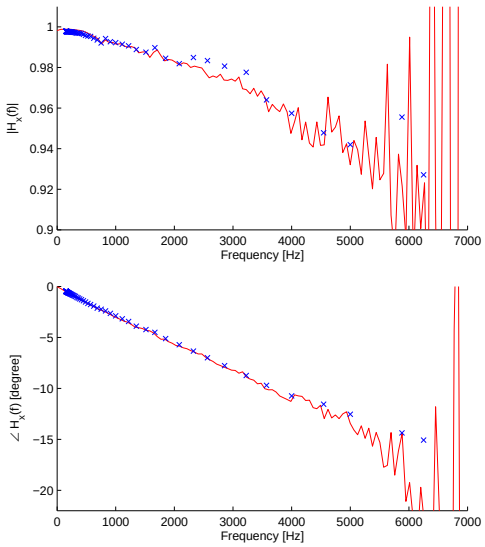

Figure 3-7: $H(f)$ calculated using a time-domain analysis of a triangle (with a gradient peak of $24mT/m$) response (*red solid*) overlaid on $H(f)$ computed using the frequency-domain analysis (*blue x*): (*top*) magnitude, (*bottom*) phase.

tude becomes quite small causing the signal to be washed out by noise. The noise is much more apparent in figure 3-7, where $H_x(f)$ was estimated using the time-domain response to a $24mT/m$ peak triangle input. The usable portion of $H_x(f)$ is where $|f| < 6000Hz$. Outside this range, $H_x(f)$ can be approximated using the same linear extrapolation and spline interpolation method performed in the frequency-domain approach.

Chapter 4

Discussion

4.1 Test waveforms

A number of different test waveform gradient inputs was used to test the validity and accuracy of the estimated transfer function $H(f)$ for each axis. Common waveform gradients were analyzed: a trapezoid gradient input on the x-axis (section 4.1.1), a spiral gradient input on the y-axis (section 4.1.2), and a echo-planar imaging (EPI) gradient input on the z-axis (section 4.1.3).

4.1.1 Trapezoid gradient input on the x-axis

The most commonly used waveform gradient is the trapezoid input. For example, this particular waveform gradient is used for the self-encode loops in the self-encode method and in the self-encoded slice selection method. In my analysis, the trapezoid gradient had a ramp up time and ramp down time of $210\mu s$ and a flat top duration of $2000\mu s$ at a gradient amplitude of $38mT/m$.

Using $H_x(f)$, the output of the ideal trapezoid input was predicted. As seen in figure 4-1, the ideal, measured, and predicted waveforms were quite similar. As seen in the close-up view in figure 4-1, the measured waveform gradient exhibited some ringing that is quite accurately predicted by $H_x(f)$. This analysis showed that the trapezoid gradient input was quite accurate, solidifying the self-encode and self-encoded slice selection algorithms.

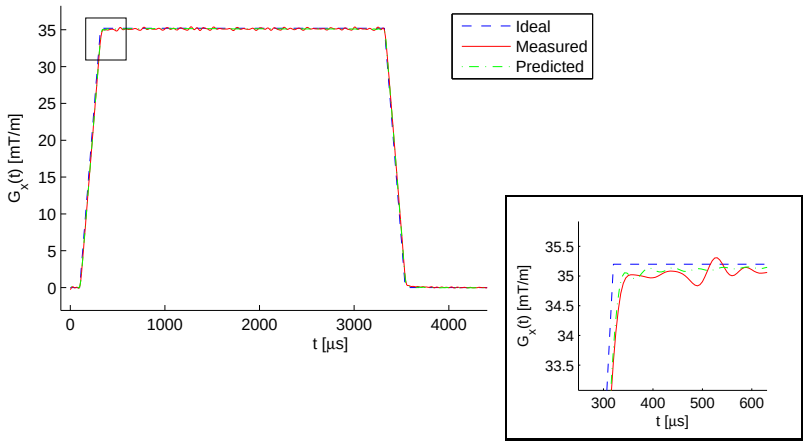

Figure 4-1: Ideal (*blue dashed*), measured (*red solid*), and predicted (*green dot dashed*) box wave gradient $G_x(t)$. Characterized on the x-axis using the self-encoded slice selection method.

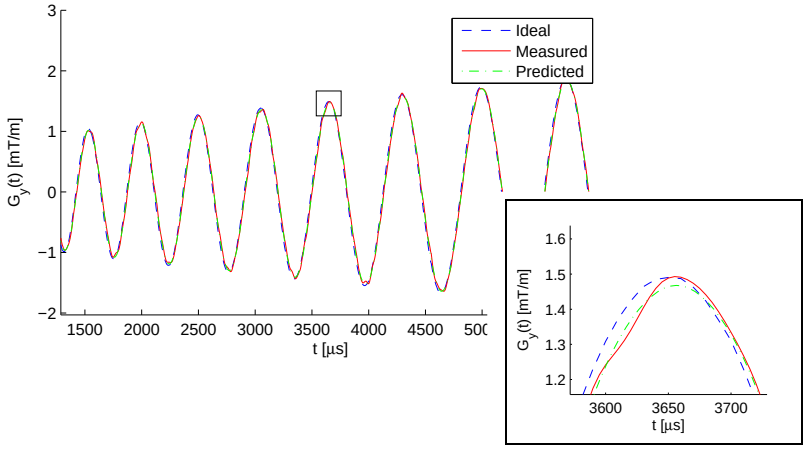

Figure 4-2: Ideal (*blue dashed*), measured (*red solid*), and predicted (*green dot dashed*) spiral wave gradient $G_y(t)$. Characterized on the y-axis using the self-encoded slice selection method.

4.1.2 Spiral gradient input on the y-axis

Spiral trajectory reconstruction requires an accurate knowledge of the k-space trajectory. Therefore, it is important to make sure that either the actual k-space trajectory is known or that the spiral waveform gradient inputs are accurate.

The spiral gradient input was analyzed on the y-axis; the result is summarized by figure 4-2. The actual waveform was very similar to its ideal counterpart. Minus the small bit of noise, the main difference between the measured waveform and the ideal waveform was the time-delay. Fortunately, the time-delay was predicted using $H_y(f)$. For this experiment, the linear phase portion of $\angle H_y(f)$ or the time-delay was sufficient enough to accurately predict the spiral waveform gradient output. From this result, the time-delay can be used to either correct the spiral gradient input or correct the k-space trajectory used for reconstruction.

4.1.3 EPI gradient input on the z-axis

A commonly used fast MR imaging technique is the EPI method. In this method, the k-trajectory quickly traverses back and forth in to acquire data in k-space. Similar to the spiral trajectory reconstruction method, the EPI method requires accurate knowledge of the k-space trajectory. For this analysis on the z-axis, the waveform gradient had a maximum gradient amplitude of $28mT/m$ and a slew rate of $168T/m/s$.

Figure 4-3 shows the EPI k-space trajectory and the corresponding waveform gradient. The measured waveform gradient had some ringing that was partially predicted by $H_z(f)$. Additionally, the time-delay was very accurately predicted. Overall, the EPI method can be more precisely executed with knowledge of the time delay.

The two figures in 4-3 emphasize the noise induced through taking a derivative, more specifically calculating $G_z(t)$ from the measured $k_z(t)$. In just looking at the k-space trajectory $k_z(t)$ (figure 4-3(a)) , the prediction was sufficiently accurate.

4.2 Gradient correction

Having knowledge of the actual k-space trajectory and gradient system transfer function naturally provides two ways of correcting gradient waveform distortion.

The first and quickest way of correcting any sort of gradient distortion is characterizing all the waveform gradients played for data acquisition. These waveforms can be either

(a)

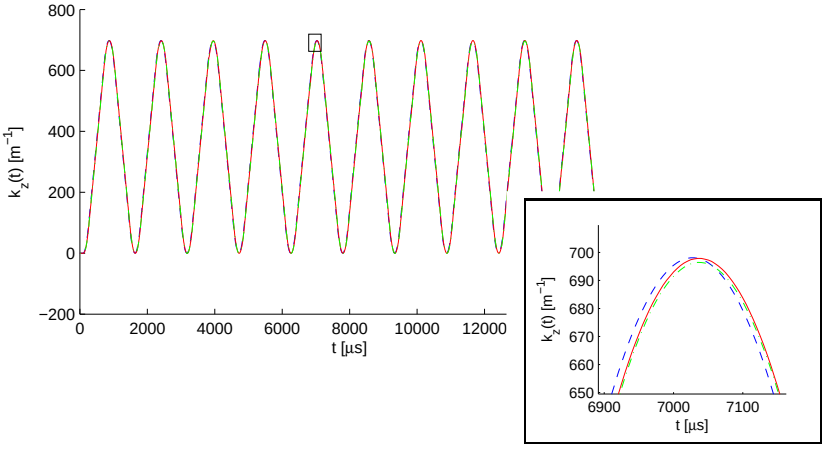

(b)

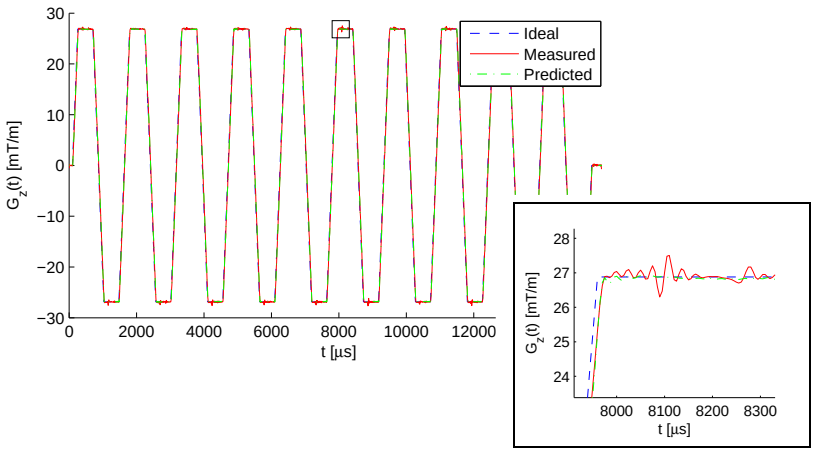

Figure 4-3: Ideal (*blue dashed*), measured (*red solid*), and predicted (*green dot dashed*) EPI wave: (a) k-space trajectory $k_z(t)$, (b) gradient wave $G_z(t)$. Characterized on the z-axis using the self-encoded slice selection method.

characterized using the self-encoded slice selection method (which require some scan time and data processing for each specific waveform) or they can be characterized by using the axis-specific $H(f)$ (which requires a one time measurement) to find a good prediction of the actual trajectory. After data is obtained for the actual scan, the data can be reconstructed with the corrected k-space trajectories. This method requires the least amount of implementation and is practical for waveforms with minimal distortion.

However, if the measured and predicted trajectories greatly differ from the ideal trajectories or if the trajectories do not even reach the desired critical k-space locations, the following approach is preferred. Using $H(f)$ estimated for the corresponding axis, the input gradient waveform can be modified to achieve the desired output. Simple Fourier-domain calculations can be performed to estimate the input necessary for a closer to ideal output. The most straightforward method is taking the Fourier transform of the ideal output and carefully dividing that ideal output by $H(f)$. One caveat is that the final input might need to be modified due to maximum gradient amplitude and maximum slew rate constraints.

For the case of the MR gradient system in the analysis, the simplest and sufficiently accurate correction is a compensation for the system's time-delay on each axis. This compensation can be done during data reconstruction by noting that the k-space trajectory associated with each data point is delayed by a factor. Or, the correction can be performed on the scanner by playing each gradient waveform earlier.

4.3 Summary

The methods of estimating the gradient system transfer function were quite robust and barely differed from measurement to measurement. Varying the maximum gradient amplitude, maximum slew rate, and the order of the sinusoid gradients characterized had no noticeable effect on the final calculated $H(f)$.

The main difference between the ideal trajectory and the measured trajectory was the time-delay factor specific to each axis, as summarized in table 3.1. There was some magnitude degradation, but the magnitude effect was very minimal.

As seen in figure 3-6 and figure 3-7, the time-domain analysis captured the time-delay quite well. If the time-delay is the main concern, the time-domain approach will be the choice of algorithm because of its speed in estimating $H(f)$. This method of calculation only

requires the characterization of only one waveform gradient. Furthermore, this approach provides sufficient knowledge of the transfer function, especially if the Fourier transform of the test waveform has mostly low frequency components.

However, the time-domain approach is prone to noise. For a more accurate representation of $H(f)$, the frequency-domain approach is preferred. Characterizing different sinusoid gradients to obtain $H(f)$ provides a very accurate and robust method of obtaining samples of $H(f)$; this can be noted by the small error bars on figure 3-3 and figure 3-4. Besides the obvious longer measurement times as compared to the duration needed for the time-domain approach, the main drawback is the fact that less and less samples of $H(f)$ can be acquired at higher frequencies (see equation 2.22). Additionally, there is also a limit for the characterizable frequency range. Theoretically, for a gradient raster time of $10\mu s$, sinusoid waveform gradients with up to a frequency of $50kHz$ can be characterized, which is a more than sufficient range for practical waveform gradients. The range is not an issue with the frequency-domain approach, only its undersampling rate of $H(f)$ at higher frequencies.

Chapter 5

Conclusion

In terms of gradient characterization algorithms, the self-encoded slice selection method is a vast improvement over the self-encode method in speed. At the same time, the algorithm allows for characterization of trajectories that push the MR system's limits in gradient amplitude and slew rate. Using the self-encoded slice selection method, estimating the gradient system transfer function becomes a much faster process in both the frequency-domain approach and the time-domain approach.

The gradient system transfer function estimation algorithms have a lot of room for improvement in terms of quality and speed. The frequency-domain approach and the time-domain approach both have their own inadequacies. The frequency-domain approach needs more samples of $H(f)$, which can be accomplished if more frequency samples (periods that are non-multiples of the gradient raster time) can be accurately obtained. For the time-domain approach, noise may be reduced through filtering or more measurements. Additionally, time-domain responses to other inputs may provide a better way of estimating $H(f)$. Since the time-domain response to a triangle gradient input characterizes a small range of frequencies, one possible solution is using a sinusoidally modulated version of the same triangle. These modulated triangles characterize different portions of $H(f)$ that can be later spliced together to form a more complete model of the transfer function.

As seen through the different experiments, the 3T Siemens Tim Trio MR scanner performs quite well in terms of waveform gradient accuracies even at the system's specified limits. As seen through the results, a simple time-delay is sufficient to correct the majority of the scanner's gradient system distortions. The time-delay can be quickly determined

using a self-encoded slice selection characterization of a short triangle gradient input.

As briefly discussed in section 4.2, the next step is correcting the distortions shown by $H(f)$ and the test waveform gradients. Through a time-domain approach, the MR scanner can be programmed to automatically obtain the time-delay and other general nonidealities with an sufficient estimate of $H(f)$. Afterward, simple corrections can be performed online using the calculated $H(f)$. Overall, the methods and analysis here present useful tools for gradient distortion correction that can be used to further push the MR system to accomplish novel tasks.

Bibliography

[1] M. T. Alley, G. H. Glover, and N. J. Pelc. Gradient characterization using a Fourier-transform technique. *Magnetic Resonance in Medicine*, 39:581–587, 1998.

[2] J. H. Duyn, Y. Yang, J. A. Frank, and J. Willem van der Veen. Simple correction method for k-space trajectory deviations in MRI. *Journal of Magnetic Resonance*, 132:150–153, 1998.

[3] A. B. Kerr. *Real-Time Interactive Magnetic Resonance Imaging*. PhD thesis, Stanford University, February 1998.

[4] D.-H. Kim and D. M. Spielman. Reducing gradient imperfections for spiral magnetic resonance spectroscopic imaging. *Magnetic Resonance in Medicine*, 56:198–203, 2006.

[5] G. F. Mason, T. Harshbarger, H. P. Hetherington, Y. Zhang, G. M. Pohost, and D. B. Tweig. A method to measure arbitrary k-space trajectories for rapid MR imaging. *Magnetic Resonance in Medicine*, 38:492–496, 1997.

[6] T. Onodera, S. Matsui, K. Sekihara, and H. Kohno. A method of measuring field-gradient modulation shapes. application to high-speed NMR spectroscopic imaging. *Journal of physics E: Scientific Instruments*, 20:416–419, 1987.

[7] D. M. Spielman and J. M. Pauly. Spiral imaging on a small-bore system at 4.7T. *Magnetic Resonance in Medicine*, 34:580–585, 1995.

[8] A. Takahashi and T. Peters. Compensation of multi-dimensional selective excitation pulses using measured k-space trajectories. *Magnetic Resonance in Medicine*, 34:446–456, 1995.